Catalysis Today 141 (2009) 385–392

Contents lists available at ScienceDirect

Catalysis Today

journal homepage: www.elsevier.com/locate/cattod

Catalytic properties of Rh, Ni, Pd and Ce supported on Al-pillared montmorillonites in dry reforming of methane

S. Barama [a,c], C. Dupeyrat-Batiot [b], M. Capron [c], E. Bordes-Richard [c,*], O. Bakhti-Mohammedi [d]

[a] Laboratoire du Gaz Naturel, Faculté de Chimie, USTHB, 16113 Alger, Algeria
[b] Laboratoire de Catalyse et Chimie Organique, CNRS-UMR 650, Ecole Supérieure d'Ingénieurs de Poitiers, 86022 Poitiers, France
[c] Unité de Catalyse et de Chimie du Solide, CNRS-UMR 8181, Université des Sciences et Technologies de Lille, 59655 Villeneuve d'Ascq, France
[d] Laboratoire de Chimie-Physique Moléculaire et Macromoléculaire, Dépt. de Chimie, Faculté des Sciences, Université de Saad Dahleb, Blida, Algeria

ARTICLE INFO

Article history:
Available online 5 August 2008

Keywords:
Dry reforming of methane
Al-pillared clay
Metal supported on clays

ABSTRACT

A natural Maghnia clay was pillared by Al_{13} and impregnated by 3–10 wt.% Me (Me = Rh, Ni, Pd, Ce) to be used as catalysts in the reforming of methane with carbon dioxide to synthesis gas. The structural and textural properties of materials calcined at 450 °C were determined by several techniques (XRD, FT-IR, ^{27}Al magic angle spinning (MAS) NMR, X-ray photoelectron spectroscopy (XPS), BET, thermogravimetric analysis (TGA)–DSC, H_2-temperature programmed reduction (TPR) and NH_3-TPR). Although impurities are present in the Al-pillared layered clay (PILC) support, most properties are close to those of pure Al-pillared Na-montmorillonite. Impregnation and calcination leads to the plugging of most micropores by clusters or microparticles of oxides. The NMR resonances of Al_{VI} and Al_{IV} specie are not modified after impregnation, and Al_{VI}/Al_{IV} ratio only varies on loading when compared to Al-PILC. Catalytic experiments show that the most active catalyst is 3% Rh/Al-PILC on which 88 mol.% of methane is converted at 650 °C with a minimum amount of carbon deposit. The conversions decrease along the 3% Rh ≈ 10% Ni > 3% Pd > 3% Ni > 3% Ce series. The H_2/CO ratio amounts to 1.1 with Rh and to 0.85 with Pd which are metallic at the temperature of reaction, but it has a lower value with Ni and Ce due to the RWGS reaction known to proceed in the presence of oxides.

1. Introduction

The dry reforming of methane by CO_2 has received much attention from both industrial and environmental aspects because it produces syngas from which synthetic fuels or alcohols can be obtained. More recently it has attracted even more attention because methane as well as carbon dioxide are harmful molecules for the greenhouse effect. One of the major problems for applying this process is the rapid deactivation of the supported metal catalyst, which is mainly due to coke deposition and sintering of both support and active metal particles. A variety of catalysts has been developed for the dry-reforming of methane [1,2] which could be the most economical way to make H_2 [3–5]. For example, a significant metal-support interaction and a strong metal–metal interaction were shown to develop in the Ni and Ni-Rh mono and bimetallic catalysts supported on ZrO_2 [6]. A series of Al_2O_3-supported Rh-Cu bimetallic catalysts was studied by Ferreira-Aparicio et al. [7] who proposed that the $CH_4 + CO_2$ reaction proceeds by means of a bifunctional mechanism. Ni catalysts have been extensively investigated owing to the metal availability and economic considerations. Recently, Ni/Mg/Al catalysts were prepared by coprecipitation method, which resulted in a higher activity of the catalysts, less coke formation and higher stability [8,9]. The high dispersion of metallic nickel strongly interacting with a basic support, and/or the addition of alkali or alkaline earth metal oxides may reduce the formation of coke [2,6,10]. The interaction between nickel and its support exerts a great effect on the reducibility of the precursor and its catalytic properties [11–13]. Recent studies indicated that NiO/MgO or NiO/Al_2O_3 catalyst, in which NiO forms a solid solution (as NiO–MgO or $NiAl_2O_4$) with the support, inhibits carbon deposition [11,14,15].

Takehira et al. [16] successfully used Ni catalysts prepared from Mg-Al hydrotalcite-like anionic clay containing Ni as the precursors. Indeed, natural silicates such as sepiolite [17,18], diatomite [19,20], and palygorskite [20,21] have recently been studied as supports owing to their potentially high acidic sites. Layered aluminosilicates clays, particularly montmorillonite and its pillared derivatives, have also been used for hydrogenation/dehydrogenation, alkylation/cracking, etc. [8,11,22–24], and they exhibit a good activity in

* Corresponding author. Tel.: +33 320434526; fax: +33 320436561.
E-mail address: Elisabeth.Bordes@univ-lille1.fr (E. Bordes-Richard).

0920-5861/$ – see front matter © 2008 Elsevier B.V. All rights reserved.
doi:10.1016/j.cattod.2008.06.025

the selective reduction of NO [25,26], as well as in wet air oxidation of organic pollutants [27].

It is well known that the method of preparation, the pore structure and morphology of the support, as well as the interactions between support and active phase may greatly influence the catalytic activity in dry reforming of methane as well as the resistance to coking. The mesoporous structure of pillared layered clays (PILCs) used to support metallic particles is favorable because, among other properties, it allows a good dispersion of metallic particles [28] and its acidity is lower than that of zeolites. A series of Me/Al-PILC catalysts varying by the amount (X = 3 or 10%) and the nature of element (Me = Ni, Rh, Pd, Ce) supported on Al-pillared clay were prepared by the impregnation method. Their structural and textural properties were examined by several methods of analysis and their catalytic properties were studied in methane reforming with CO_2.

2. Experimental

2.1. Catalysts preparation

Catalysts called X% Me/Al-PILC were prepared with X = 3, 5 and 10% of Me = Ni, Rh, Pd, Ce, supported on Al-pillared clay. The support was prepared starting from raw Maghnia-bentonite clay (''Roussel'' mine of Maghnia, Algeria). Its composition (in wt.%) of the calcined clay is SiO_2 (67.7), Al_2O_3 (20.0), MgO (3.9), Fe_2O_3 (3.8), TiO_2 (0.3), CaO (1.2), K_2O (1.5), Na_2O (1.5), MnO (0.08), P_2O_5 (0.06) [29]. After sifting the clay with 1.60 mm-sifter followed by fast grinding by the 4-knives-grinder SM100 down to the 0.25 and 0.63 mm fraction, the clay was purified by washing several times with distilled water to eliminate the surface impurities. The montmorillonite fraction was obtained by sedimentation of 400 g of Maghnia-bentonite clay in 500 ml of water saturated with 1 M NaCl solution to obtain the homoionic compound. Finally, the sodic bentonite was obtained by washing up to constant conductivity, followed by centrifugation at 3000 rpm during 15 min. The cation exchange capacity of this clay determined from the ammonium exchanged (micro Kjeldhal method) was 90 meq/100 g. The aluminium intercalated clay Al-PILC was prepared by addition of the Keggin oxyhydroxyaquo aluminium $[Al_{13}O_4(OH)_{24}(H_2O)_{12}]^{7+}$ cation (shortened as Al_{13}). The intercalating Al_{13} solution was first prepared by titration of $AlCl_3{\cdot}6H_2O$ 0.1 M with NaOH 0.2 M at 70 °C until the OH/cation molar ratio was equal to 1.8 [30]. It was added to the clay suspension in water (5 wt.%) under vigorous stirring. The final Al/clay ratio was 4 mmol/g of dry clay. After ageing at pH 11.8 for 24 h, the pillared clay precursor was washed until total elimination of chloride ions, dried at 70 °C during 24 h and finally calcined at 450 °C for 4 h.

The supported metallic catalysts were prepared by conventional wet impregnation method, using aqueous solutions of metallic nitrates (Ni, Rh, Ce) or palladium chloride 0.1 M. The clay particles were added into the solution of metallic salt at the desired concentration, and heated under stirring to evaporate water. The solid residue was dried at 105 °C overnight and calcined at 450 °C in air during 4 h.

2.2. Physicochemical analysis of catalysts

The X-ray diffraction of catalyst powders was carried out on BRUKER D5005 diffractometer with Cu Kα radiation. FT-IR spectroscopy was performed on a PerkinElmer instrument (GX/FT-IR system) between 200 and 4000 cm^{-1} using KBr-sample discs. The ^{27}Al solid-state NMR experiments were carried out on ASX Bruker ASX400 (9.4 T) spectrometers operating at ^{27}Al Larmor frequencies 104.3 MHz using 3.2 mm magic angle spinning (MAS) probeheads. The ^{27}Al MAS NMR spectra were recorded at spinning rates of 20 or 14 kHz using a single pulse excitation sequence with small pulse angle ($\pi/12$) to ensure a quantitative excitation of the central transition [31] and recycle delay of 4 s. The ^{27}Al triple-quantum MAS (3Q-MAS) spectra [32] were recorded at 9.4 T using the t_1 rotor-synchronized z-filtered pulse sequence [33]. The first two hard-pulse lengths were 2.75 and 1 μs, and the third soft 90° CT pulse length was 21 μs. The recycling delay was 0.5 s and 56 slices were recorded at a spinning speed of 14 kHz. The resonances of the sheared MQ-MAS spectrum are labelled by their normalized ppm coordinates [34] on the MAS δ_{MAS} and isotropic δ_{iso} axes, respectively. The ^{27}Al chemical shifts were referenced at 0 ppm relative to an $Al(NO_3)_3$ 1 M aqueous solution. X-Ray photoelectron spectroscopy (XPS) was performed on VG-ESCALAB 220XL spectrometer. The Al Kα monochromatized line (1486.6 eV) was used at 120 kV (500 μm spot diameter). The powder samples were pressed in a 2 mm hole on a steel block. The spectrometer was operated in a constant pass energy mode (E_{pass} = 30 eV) at a pressure less than 10^{-7} Pa. Experimental quantification level and spectral simulation were obtained using the Eclipse software provided by VG Scientific.

The textural properties were determined by BET method using N_2 at 77 K with TRISTAR 3000 and isotherms were obtained on ASAP 2000 MICROMERITICS. Depending on the density of the material, 0.04–0.18 g were outgassed at 250 °C during 30 min. The morphology of particles and their composition were obtained by scanning electron microscopy (SEM) (Hitachi 4100S) equipped with EDX. The thermogravimetric analysis (TGA/DSC) was carried out on Setaram 92 microbalance in air at 10 °C min^{-1} heating rate up to 900 °C. The reducibility of samples was studied by temperature programmed reduction (TPR) using Micromeritics Autochem 2910 with a TCD detector to monitor the H_2 consumption. After calibration of hydrogen on the TCD, the sample displayed in a U-shaped quartz reactor was pre-treated in Ar up to 120 °C, and heated at 5 °C min^{-1} from 20 to 800 °C in 3 vol.% H_2/Ar at 5 ml/min flow rate. The temperature-programmed desorption of NH_3 (NH_3-TPD) was carried out between 20 and 600 °C in the same apparatus. Prior to adsorption, the sample (0.08–0.1 mg) was treated at 400 °C for 3 h in helium flow (50 cm^3 min^{-1}), cooled down to 30 °C and then treated for 30 min in 10% NH_3/He. Desorption was carried out at 10 °C min^{-1} 1 in He flow.

2.3. Catalytic testing

The oxidation of CH_4 with CO_2 was conducted using a fixed-bed flow quartz reactor with on-line analysis of effluents by mass spectrometry. Five hundred milligrams of catalyst powder were displayed in the reactor and equilibrated for 2 h in CH_4/CO_2/He = 10/10/80 gas flow while increasing temperature (5 °C min^{-1}) up to 750 °C. The catalytic operating conditions were CH_4:CO_2:He = 10:10:80, at total flow rate F = 12 l h^{-1} (W/F = 83 h l^{-1} $g_{cat}{}^{-1}$), temperature 550–750 °C, at atmospheric pressure. Signals of $H_2{}^+$, CO^+, $CH_3{}^+$ and $CO_2{}^+$ (q/m = 2, 28, 15, 44, respectively) were used to calculate the conversion of methane and of CO_2 and the selectivities to H_2 and CO. Carbon deposited on catalysts was chemically analysed by the Service Central d'Analyses of CNRS (France).

3. Results and discussion

3.1. Characterization of the precursor (Al-PILC) and of catalysts

The XRD pattern of the Maghnia Na-bentonite clay after pillaring by Al (Al-PILC) and calcination at 450 °C shows that some lines of quartz (Q) and kaolinite $Al_2Si_2O_5(OH)_4$ (K) are present

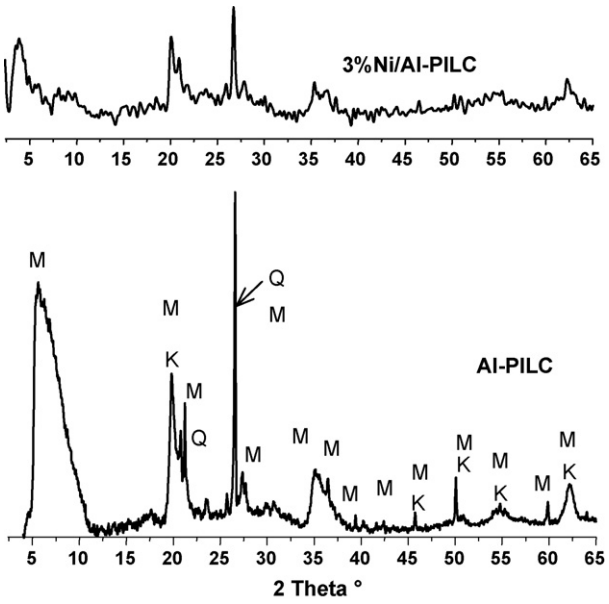

Fig. 1. XRD patterns of Al-PILC and of 3% Rh/Al-PILC after calcination (M: montmorillonite; K: kaolinite 1A; Q: quartz).

besides the lines characteristic of montmorillonite (Fig. 1). The interlayer spacing $d_{0\,0\,1}$ of montmorillonite particles increases from 1.00 before to 1.75 nm after Al-pillaring and calcination. Depending on methods of preparation, higher values of $d_{0\,0\,1}$ are often found for Al-PILC [27], up to 1.86 nm for Al-PILC [35], but after calcination they reduce to 1.8–1.7 nm [36]. The Keggin-type Al_{13} oligomer which is the constituent of the pillars is made up from one four-fold coordinated aluminium sharing faces and corners with 12 six-fold coordinated Al. Its size is responsible for the $d_{0\,0\,1}$ spacing in pillared clays. The impregnation of Al-PILC by aqueous solutions of Ni^{2+}, Pd^{2+}, Rh^{3+} cations followed by calcination does not lead to strong variation of the patterns except the $d_{0\,0\,1}$ spacing which decreases (3% Ni) or even disappears (Pd, Rh). The disappearance of the (0 0 1) line means that the material has a delaminated structure (non parallel ordering of the clay layers). No line of Me oxides is observed except the $d_{2\,0\,0}$ = 0.203 nm of NiO in 10% Ni/Al-PILC. The interlayer spacing increases slightly in the case of Ce/Al-PILC ($d_{0\,0\,1}$ = 1.77 nm). At variance with Fe^{3+} (when added on purpose) which can compete with Al^{3+} for isomorphous substitution, cerium can generate a Ce-Al_{13} polycation and thereby it may contribute to the building of pillars [28,29,37]. The comparison by SEM of particles of Al-PILC, 3% Ni/Al-PILC and 10% Ni/Al-PILC particles shows that the mean size of Al-PILC particles is smaller than after impregnation by Ni and that it increases with the loading of Ni, in accordance with the decrease of the specific surface area.

The FT-IR spectrum of Me-impregnated Al-PILC catalysts does not change much compared to that of Al-PILC. Two strongly intense bands at 3620 and 3425 cm^{-1} are assigned to the fundamental stretching modes of hydroxyls bound to silica and to clay lattice, and the deformation of OH of water occurs at 1629 cm^{-1}. The pillared montmorillonite being mainly composed of silicate chains (–SiO_4–), the Si–O stretching band at 1044 cm^{-1} is related to crystalline silica admixtures. The influence of Al incorporated in the structure of PILC is accounted for by bands at 522 and 466 cm^{-1} which are characteristic of Al–O–Si and Si–O–Si deformation vibrations, respectively. The presence of bands at 714 cm^{-1} (Al_{IV}–O), 634 cm^{-1} (Al–OH), 568 cm^{-1} (Al_{VI}–O) and 483 cm^{-1} (Al–OH_2) assigned to Al_{13} [38] cannot be ascertained because the spectrum is not well resolved in this range.

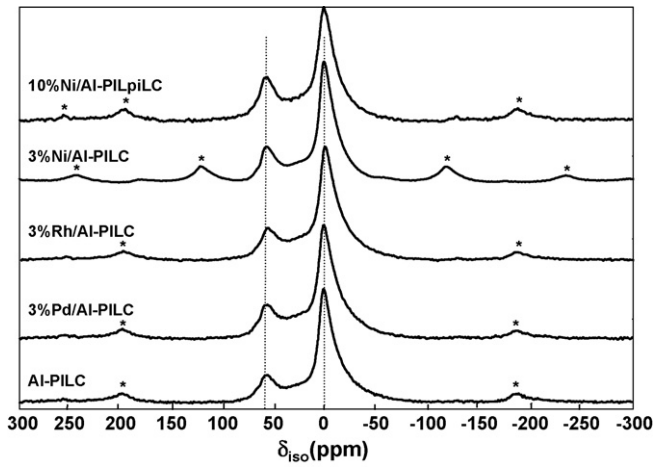

Fig. 2. ^{27}Al MAS NMR of Al-PILC support and Me/Al-PILC catalysts after calcinations.

^{27}Al MAS NMR spectroscopy reveals that several Al specie are present in raw and impregnated Al-PILC (Fig. 2). The ^{27}Al MAS spectra of Al-PILC consists of at least two overlapping resonances with two maxima located in the range of four- and six-fold coordinated aluminium Al_{IV} and Al_{VI}, respectively, as discussed below. The two kinds of resonance, as well as the broad band at ca. 20 ppm are observed in the spectrum of Al-PILC and all Me/Al-PILC catalysts. Kaolinite as well as montmorillonite are typical dioctahedral clays [39] with formula $[Si_{8-x}M_x]^{IV}[Al_{4-y}M'_y]^{VI}(OH)_4O_{20}M''^{n+}_{(x+y)/n}\cdot mH_2O$, where the charge of M and M′ is one unit less than the substituted cation and M″ is the exchangeable cation. In Na-montmorillonite, isomorphous substitution of Mg^{2+} for part of the Al^{3+} is observed and a small part of Al is tetrahedral and binded to Si according to the formula $[Na_{0.38}Ca_{0.03}Mg_{0.01}][Si_{3.86}Al_{0.14}]^{IV}[Al_{1.59}Fe_{0.1}Mg_{0.31}]^{VI}(OH)_2O_{10}\cdot mH_2O$ (Al_{VI}/Al_{IV} = 11.4). Plee et al. [36] gave the formula $Na_{0.0.6}Al^{(13)}{}_{1.65}Si_8[Al_{3-}Fe_{0.35}Mg_{0.65}]^{VI}O_{24.2}$ for an Al-pillared Wyoming montmorillonite, where $Al^{(13)}$ represents one Al atom in one hydroxy polymer unit. The impregnation step by 3% Me^{n+} followed by calcination does not seem to alter significantly the environment of aluminium. However for quantification it is necessary to get better insight of the shape of the resonance, and a MQ-MAS experiment was performed on 3% Ni/Al-PILC, enabling to separate two different sites. The resonance of Al_{IV} located at an isotropic chemical shift δ_{iso} = 58.8 ppm is well defined without distribution, and it can be simulated with a symmetrical shape close to a Gaussian line (Fig. 3). The second resonance located in the Al_{VI} isotropic chemical shift range with a distribution of quadrupolar constant (i.e., the resonance is along the δ_{QIS} line) was simulated using the Czjzek model [40] in the DM fit program [41]. This model, often used to simulate MAS experiments for quadrupolar nuclei in glassy, amorphous and disordered materials, describes the structural disorder around the probe nucleus at the two or three atomic positions scale which results from a variation of the quadrupolar interaction (variation of the electronic field gradient). Using the shape determined with the MQ-MAS experiment, the ^{27}Al MAS spectra of the Al-PILC series have been fitted. Fig. 3 presents a typical fit in the case of 10% Ni/Al-PILC representative of the full series and data obtained for other catalysts using the same resonances are gathered in Table 1. If only two resonances evidenced with the MQ-MAS experiment are introduced in the model, the spectrum cannot be correctly fitted, and a third line located at approximately 16.8 ppm must be introduced. This resonance does not appear in the MQ-MAS experiment due to its fast decrease relaxation in the 3Q. This phenomenon can be due to

Table 1
Quantification of ^{13}Al MAS NMR resonances for the Al-PILC support and impregnated Me/Al-PILC catalysts

Catalyst	Al_{VI}	Al_{IV}	"Al_V"	Al_{VI}/Al_{IV}	$Al_{VI} + Al_V/Al_{IV}$
Al-PILC	60.4	14.5	25.1	4.2	5.9
3% Ni/Al-PILC	62.4	17.1	20.5	3.7	4.9
10% Ni/Al-PILC	50.1	21.1	28.8	2.4	3.7
3% Rh/Al-PILC	53.5	14.9	31.6	3.6	5.7
3% Pd/Al-PILC	52.3	15.9	31.8	3.3	5.3

δ_{iso} Al_{IV} = 58.8 ppm; δ_{iso} Al_{VI} = 8.8 ppm; δ_{iso} "Al_V" = 16.8 ppm.

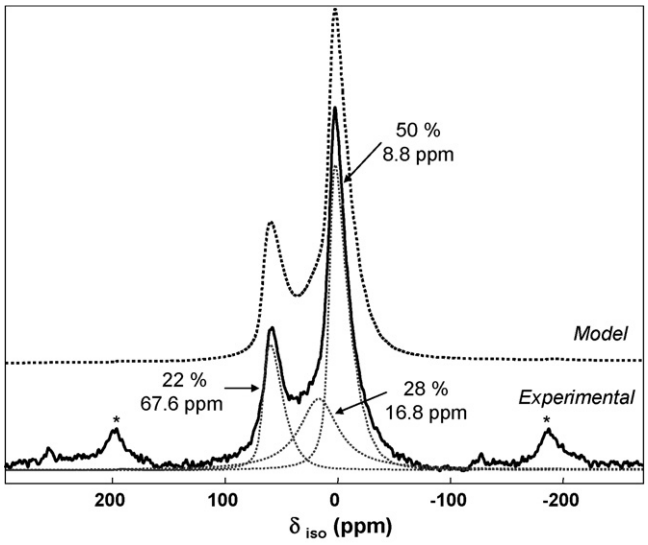

Fig. 3. ^{27}Al MAS spectrum of 10% Ni/Al-PILC (full line: observed spectrum; dotted lines: deconvoluted pattern).

a broad line resulting from an asymmetric environment of this type of Al, and thus the geometry around the aluminium atoms may be distorted octahedral or pentahedral. The impregnation and calcination steps do not modify the environment of Al but they do modify the amount of Al_{VI} in the samples as shown by the value of the ratio between Al specie (Table 1). The Al_{VI}/Al_{IV} ratio is lower than expected (Al_{VI}/Al_{IV} = 11.4 in Na-montmorillonite and 12 in Al_{13}), as well as when pseudo octahedral specie are taken into account ($Al_{VI} + Al_V/Al_{IV}$ ratio). This is particularly observed with 10% Ni/Al-PILC, in which case the amount of octahedral Al present in Al-PILC strongly decreases, as Al_{VI}/Al_{IV} and Al_{VI}/Al_V are 35 and 43% lower, respectively, compared to 3% Ni (Table 1). The values of δ_{iso} for Al_{IV} and Al_{VI} are at ca. 59 and 8.8 ppm, respectively. Typical values of δ_{iso} for tetrahedral Al in Al_{13} pillared clays are at ca. 56 and 67 ppm, respectively in synthetic pillared hectorite after calcination at 400 °C, and 63–67 ppm for pure dried Al_{13} salts [35]. The first value (56 ppm vs. 59 ppm) seems to confirm the presence

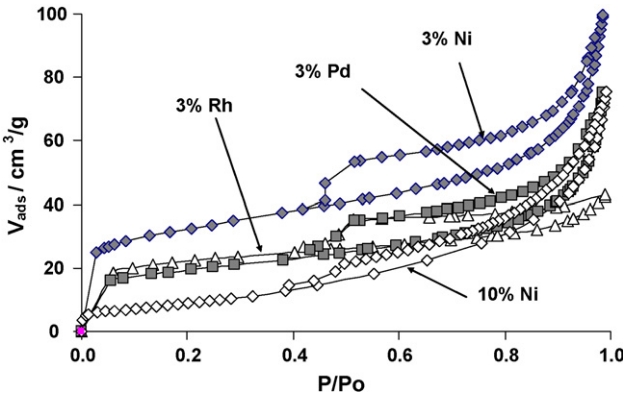

Fig. 4. Adsorption isotherms of 3% Ni, 3% Rh, 3% Pd and 10% Ni supported on Al-PILC.

of Al_{13} pillars in our materials. The ^{27}Al δ_{iso} in crystallized γ-alumina (spinel) are 76 and 14.5 ppm for Al_{IV} and Al_{VI}, respectively, and the ratio Al_{VI}/Al_{IV} can vary from 1.33 to 1.5. These values are far from ours so that the formation of γ-alumina particles can be discarded.

Table 2 presents the values of specific surface area (BET method) and volumes and surfaces of micro and mesopores extracted from nitrogen adsorption/desorption isotherms. The BET N_2 method requires a complete initial degassing of the materials, and this pulls the lamellae together in such a way that they are not "intercalated" by N_2. It is known that the surface area and pore volumes are better determined by adsorption of water or, e.g., cetyl pyridinium in aqueous solution [42,43]. Keeping that in mind, the volume of micropores has been evaluated by the *t*-plot method. The adsorption isotherm with hysteresis is typically Type IV corresponding to mesopores, but at low values of p/p° it is close to Langmuir (Fig. 4). Both micropores and mesopores are present in pillared clays, the first being associated with the pillared sheets as microcrystals and the second with the random arrangement of these microcrystals [38], unless they are synthetic (more crystalline) pillared montmorillonites. The BET specific surface area of the Al-PILC support (229 m^2/g) is lower than that obtained in many papers (270–250 m^2/g). The presence of kaolinite and quartz may also be responsible for that. The total micropore volume is in the range 0.13–0.15 cm^3/g [36,43–45]. After impregnation the BET specific surface area of the calcined catalysts is significantly lower than that of Al-PILC calcined support. It decreases along 3% Ni (113) > 3% Ce (81) ≈ 3% Rh (79) > 3% Pd (67) > 10% Ni (32 m^2/g) series. Such a decrease is generally observed, as, e.g., in the case of Cu^{2+} or Co^{2+} cations in Al-pillared montmorillonite [45]. Most of the total volume is due to mesopores, at variance with literature, but it explains the lower BET surface area and the shape of isotherms. For all catalysts the pore diameters obtained by BJH are larger than 50 nm, thus the initial mesoporosity of Al-PILC changes to become macroporosity. Therefore the solids have undergone a modification owing to the incorporation of the transition elements.

Table 2
Textural characteristics of Al-PILC and impregnated catalysts after calcination

Catalyst	BET surface area (m^2/g)	External surface area (m^2/g)	Total pore volume[a] (cm^3/g)	Micropore surface area (m^2/g)	Micropore volume (cm^3/g)
Al-PILC	229		–	–	–
3% Ni/Al-PILC	113	70.1	0.148	42.9	0.0193
10% Ni/Al-PILC	32	31.7	0.102	11.8	0.0053
3% Rh/Al-PILC	79	43.4	0.064	36.8	0.0157
3% Pd/Al-PILC	67	43.6	0.106	23.7	0.0108
3% Ce/Al-PILC	81	93.1	0.108	44.0	0.0201

[a] p/p° = 0.9814.

Table 3
Binding energies (BEs, eV), atomic percentage and atomic ratios obtained from XPS experiments performed on Al-PILC and nickel supported on Al-PILC

Catalyst	Al 2p		Si 2p		C 1s		Ni 2p		Al/Si	Ni/Al
	BE	At.%	BE	At.%	BE	At.%	BE	At.%		
Al-PILC	74.9	12.9	102.8	21.8	285.0	5.1	–	–	0.59	–
3% Ni	75.0	13.5	102.9	19.0	285.1	6.5	856.9	1.9	0.71	0.14
10% Ni	74.7	12.0	102.8	16.4	285.1	9.3	856.2	5.9	0.73	0.49

BE O 1s: 532.2–532.1 eV.

Table 4
Temperature of the first endotherm and at the maximum rate of the second and third losses of weight (TGA/DSC in air) support and catalysts

Catalysts	1st step	2nd step		3rd step	
	Temperature[a] (°C)	Temperature (°C)	Rate ($\times 10^{-3}$ wt.%/°C)	Temperature (°C)	Rate ($\times 10^{-2}$ wt.%/°C)
Al-PILC	113	402	5.77	615	1.34
3% Ni/Al-PILC	96	360	9.20	592	1.71
10% Ni/Al-PILC	98	340	3.21	590	1.40
3% Rh/Al-PILC	102	330	4.26	620	1.75
3% Pd/Al-PILC	98	380	4.33	633	1.39
3% Ce/Al-PILC	107	408	5.90	625	1.50

[a] First endotherm.

Supposing that the nature of the counter anion of Me (nitrate or chloride) has little effect, two phenomena may explain this strong decrease. The first is due to the impregnation step (ion exchange). Adding Me^{n+} cations to Al-PILC particles results mainly in the plugging of micropores, but leaving open the mesoporosity (type IV for all isotherms). Very small particles of oxides (not detected by XRD, except for 10% Ni) have blocked the interlayers of Al-PILC and are probably displayed on the surface (sheets and edges). For example, the micropore volume is divided by four on increasing the loading of Ni from 3 to 10% Ni. Moreover partial hydrolysis may occur leading to the partial collapse of the pillars, with or without leaching of, e.g., Al_{VI}^{3+}. This would explain why the ratio between octahedral and tetrahedral Al specie (Al_{VI}/Al_{IV}) calculated from NMR data (Table 1) is so low (Al_{VI}/Al_{IV} = 2.5–4.2 instead of 11–12). Second, during calcination at 450 °C, the loss of water molecules and partly of hydroxyls leads to a partial collapse and cross-linking of the pillars, which is related to the decrease of the basal spacing $d_{0\,0\,1}$ (XRD). Indeed the micropore volume decreases along 3% Ce ≈ 3% Ni > 3% Rh > 3% Pd ≫ 10% Ni. The isomorphous substitution of Me^{n+} in sheets or pillars is uncertain due to their ionic radius or coordination (case of usual square coordination of Pd). The ionic radius increases along Ni_{VI}^{2+} 0.600 Å < Pd_{IVsq}^{2+} 0.640 Å < Rh_{VI}^{3+} 0.665 Å < Pd_{VI}^{2+} 0.860 Å < Ce_{VI}^{4+} 0.870 Å, compared to those of PILC constituents (Al_{VI}^{3+} 0.535 Å < Fe_{VI}^{3+} 0.645 Å < Mg_{VI}^{2+} 0.720 Å. However Ce^{4+} is known to stabilize pillars as shown with $d_{0\,0\,1}$ = 1.77 nm, and Ni^{2+} could substitute Al_{VI}^{3+}, Fe^{3+} or Mg^{2+}.

The binding energy (BE) and composition in the ca. 1 nm-depth of Al-PILC and 3 or 10% Ni/Al-PILC determined from XPS experiments are presented in Table 3. In Al-PILC the presence of expected elements (Al, Si, O) plus Mg (0.64 at.%) but except iron is observed. A small amount of fluor (0.64 at.%) which is an impurity that may come from kaolinite or during the formation of sodium montmorillonite is also noted. Typical BEs are 102.75 eV (Si $2p_{3/2}$), 74.8 eV (Al $2p_{3/2}$), 532 eV (O 1s) in montmorillonite and 102.45 eV (Si $2p_{3/2}$), 74.3 eV (Al $2p_{3/2}$), 531.5 eV (O 1s) in kaolinite (carbon C 1s reference) [46]. The percentage of Si decreases and carbon increases in pillared clay along Al-PILC < 3% Ni < 10% Ni. The BE of nickel $2p_{3/2}$ is higher by 2 eV than for NiO (853.5–854.2). The Al/Si and Ni/Al ratios both increase in the same series. The value of Ni/Al changes (0.14/0.49 = 0.28) in the same way than Ni loading (3/10 = 0.3). Thus XPS shows that most nickel is displayed on the surface of Al-PILC.

The stability of the raw and impregnated Al-PILC support solids was studied by TGA/DSC in air up to 850 °C. Three losses of weight are observed for calcined Al-PILC (Table 4). The first one ends at ca. 220 °C and corresponds to the endothermic peak at 95–110 °C (Fig. 5). It accounts for the loss of physically adsorbed water, as expected from a micro/mesoporous compound and it is known to depend on the nature of exchangeable cations [9]. Between 220 and 500 °C, there is a slight decrease of weight, meaning that hydration water and hydroxyl groups are slowly but continously expelled. That second step is assigned to the loss of OH, H_2O from pillars. Remarkably Al-PILC and 3% Ce/Al-PILC behave quite in the same way as compared to other catalysts. A broad endothermic peak (550–650 °C) accounts for full dehydroxylation which is about twenty-times faster than for the second step. Little variation of rate is observed when considering all the catalysts (1.3–1.7 × 10^{-2} wt.%/°C). The last endothermal signal corresponds to the collapse of the PILC structure, which is known to be followed by recrystallisation of silica at higher temperature [39,42,45].

The catalyst reducibility was examined by H_2-TPR (Fig. 6). Al-PILC profile exhibits a small and broad peak centered at 345 °C that can be attributed to the reduction of Fe^{3+} because it is the only reductible element in PILC. Two main peaks of reduction are observed for Rh, Pd and Ni supported on Al-PILC. At the lowest temperature, the first peak accounts for the reduction of specie which are poorly anchored onto Al-PILC surface. The temperature

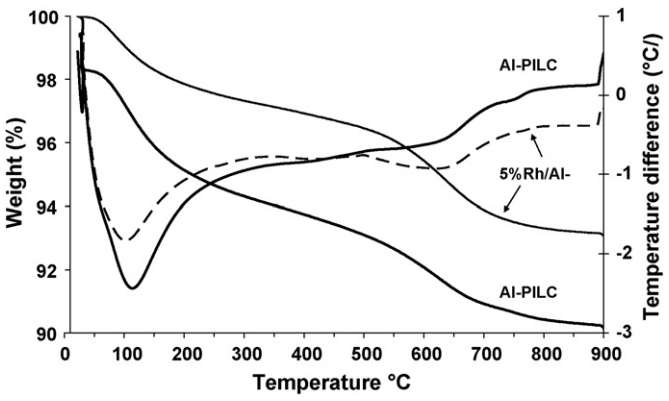

Fig. 5. TGA/DSC of Al-PILC and 3% Rh/Al-PILC heated in air.

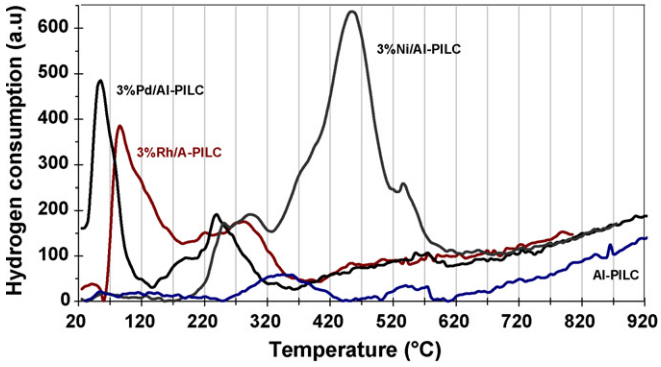

Fig. 6. H_2-TPR profiles of Al-PILC, 3% Rh 3% Pd and 3% Ni, all supported on/Al-PILC (signals not normalized by weight of sample).

increases along Pd^{2+} (→ Pd, 50 °C) < Rh^{3+} (→ Rh, 90 °C) < 3% Ni^{2+} (→ Ni, ca. 250 °C), in accordance with the known reducibility of the cations. A plateau (Rh) or a second peak (Pd) are observed at 220–270 °C and they account for specie more firmly held on the surface of Al-PILC particles. Several Ni specie are present in 3% Ni/Al-PILC as shown by the multicomponent peak between 230 and 620 °C. The more labile specie appear in the same temperature range (230–320 °C) than for Rh and Pd. The specie strongly bonded to Al-PILC at ca. 540 °C are very probably located inside the structure (isomorphous substitution). In between (T_{max} = 465 °C), specie belong to clusters and microparticles of NiO anchored in the support. It is interesting to note that all these specie are more easily reduced than when they are supported on an oxide like MgO (ca. 600 °C) [12,47]. However in the latter case the main explanation could be that the structure of MgO is far more compact than that of Al-PILC is.

The TPD of ammonia provides a measure of both Brönsted and Lewis acidity. The amount of desorbed ammonia is taken as a measure of the acid sites concentration while the temperature range indicates the strength of the acid sites. On Al-PILC, the chemisorption of ammonia takes place mainly on the surface of Al pillars and of montmorillonite layers. It is widely accepted that Lewis acidity is strongly related to the number and composition of the pillars, while a weak Brönsted acidity arises from structural hydroxyl groups of montmorillonite layers. The NH_3 desorption pattern of Al-PILC, Ni/Al-PILC and Ce/Al-PILC consists of three unresolved maxima, while a peak is also observed in the case of Rh and Pd/Al-PILC (Table 5). In all samples but cerium the majority of NH_3 molecules (about 40%) desorbs between 200 and 300 °C. The total acidity increases along the Pd ≪ Al-PILC < Rh < 3% Ni < 10% Ni < Ce series, and it is the same order when acidity is calculated at T < 300 °C (to get rid of the oxidation of NH_3). It is quite independent of the surface area which increases along 10% Ni < Pd < Rh ≈ Ce < 3% Ni < Al-PILC. The amount of adsorbed ammonia on Al-PILC (ca. 330 μmol/g_{cat}) is close [36,48] or lower [49] than values obtained in literature by the same method. Upon calcination, the crosslinking pillars and silica layers of the clay induce the formation of stronger Lewis and new Brönsted sites [50]. The comparison with Ni catalysts shows that more acid sites are generated on Ni loading, with a regular increase at all temperatures. At variance with other catalysts, cerium brings a lot of strong acid sites which are probably of Brönsted type since the maximum is observed at low temperature. In the case of montmorillonite pillared with both Al and Ce, it was noted that they present not only a greater acidity than Al-PILC but also a greater number of strong acid centers [36]. In the case of Rh and Pd, a more (Rh) or less (Pd) sharp peak is observed at 305–310 °C, which accounts for the oxidation of NH_3 to N_2 as shown in literature for silver [26]. Like nickel in our case, this reaction was not observed with copper or cobalt-supported on Al-PILC [44]. Therefore it is probable that small particles of PdO and Rh_2O_3 have been reduced by ammonia and that the resulting metallic particles become active in the oxidation of NH_3. As Pd and Rh are the more easily reduced among Me/Al-PILC, this would be in accordance with H_2-TPR results.

3.2. Catalytic reactivity in methane reforming with CO_2

The catalytic reactivity of Me/Al-PILC was examined in the dry reforming of methane. The main reaction is usually accompanied by several secondary processes, reverse water-gas shift (RWGS) being the main one and Boudouard reaction (reversible conversion of CO to CO_2) one of the others. The major obstacle of dry reforming

Table 5
Acidity (μmol $NH_{3\ ads}/g_{cat}$) determined by adsorption of ammonia as a function of temperature for Al-PILC support and catalysts

Adsorbed NH_3 (μmol/g_{cat})	T_{max}[a] (°C)	Temperature range (°C)			Total ads. NH_3 (μmol/g_{cat})
		40–70	200–300	300–600	
Al-PILC	42 246 587	27.5	277.5	23.2	328
3% Ni/Al-PILC	43 229 580	52.4	351.6	87.8	492
10% Ni/Al-PILC	44 211 571	68.8	358.6	152.3	580
3% Rh/Al-PILC	48 276	32.8	365.4	0.0	398
3% Pd/Al-PILC	39 226 333 595	48.3	92.9	44.2	186
3% Ce/Al-PILC	65 256 640	308.3	159.8	68.6	537

[a] Temperature at maximum of adsorption.

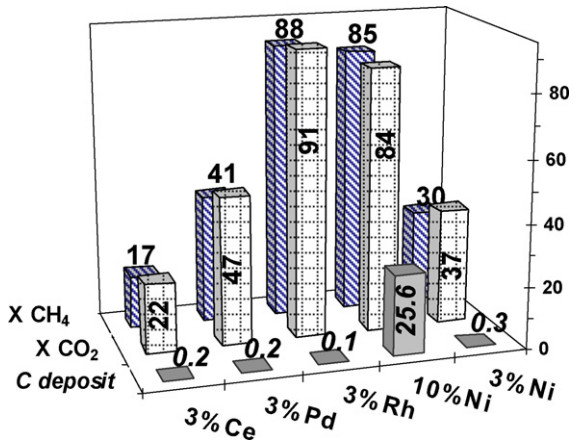

Fig. 7. CO_2 reforming of methane on catalysts: conversion of methane and of carbon dioxide (mol.%) at 650 °C, and amount of carbon deposited (wt.%) on catalyst from element analysis.

is the carbon deposition on catalysts surface which is related to the acidity of the support. This is the reason why basic oxides have been tested as supports [9,12,16].

The trend followed by the conversions of methane X_{CH_4} and of carbon dioxide X_{CO_2} is parallel, and conversions are high with Rh (ca. 90 mol.%) and 10% Ni (ca. 85 mol.%) at 650 °C. Other catalysts are less active. The conversion of both reactants decrease along Rh ≈ 10% Ni ≫ Pd > 3% Ni ≫ Ce series (Fig. 7), and it does not follow the trend of surface areas (10% Ni < Pd < Rh ≈ Ce < 3% Ni). The H_2/CO ratio amounts to more than 1.0 only with Rh and it decreases along Rh (1.11) > Pd (0.84) ≫ Ni, Ce (0.12–0.05). Values lower than 1.0 are due to RWGS which is generally observed in the presence of oxides. Small amounts of coke are observed except in the case of 10% Ni/Al-PILC, one of the two highly active catalysts.

Therefore the oxidic and/or metallic form of particles on the surface of Al-PILC is worth examining. To decide on that state it should be necessary to examine the catalysts after reaction and to apply a reduction pre-treatment, both experiments not yet performed. However the chemical nature of the oxidic particles is very different as revealed by the analyses just exposed. The higher acidity is found for Ce/Al-PILC but Ce is not active for the reaction, may be owing to the easy formation of carbonates. Ni catalysts exhibit also a high acidity. The difference of activity vs. loading may be related to the number and size of Ni(O) particles. The acidity of Rh and Pd supported is the lowest, but these specie being able to oxidize ammonia are certainly present in the metallic state. The H_2-TPR experiments are also in favor of this hypothesis because both Rh and Pd are reduced at very low temperature. Ni and Ce are probably partly reduced to Ni^0 and Ce^{3+}. One could expect that the trend of reducibility obtained by H_2-TPR (Pd > Rh > Ni) would be parallel to that of methane and CO_2 conversion or H_2/CO during catalysis. Therefore and as expected the precious metals are far more active and selective to hydrogen than Ni and Ce. Palladium must be partly responsible for the formation of high amounts of hydrogen, while maintaining a low coke formation (0.17 wt.% of the catalyst) in accordance with its low acidity.

4. Conclusion

Although impurities and foreign phases (e.g., kaolinite) are present besides montmorillonite after pillaring by Al_{13}, the results show that most properties of calcined Al-PILC are similar to those of literature. After impregnation by cationic solutions (Me^{n+}) followed by calcination which leads to a certain degree of cross-linking and collapse of pillars, the surface area decreases due to the plugging of micropores. Thermal analyses show that the nature of cations exerts a moderate influence on the rate of loss of water and of hydroxyls from the pillars. ^{27}Al MAS NMR shows that the ratio of octahedral to tetrahedral aluminium specie is different from what could be expected, although the real composition of such materials is difficult to know. However the chemical shifts do not account for the presence of γ-alumina. Therefore it can be inferred that small oxidic clusters are well dispersed on the surface of pillars and sheets. Part of Ni^{2+}, Ce^{3+} may be incorporated in the Al-PILC structure but XPS of Ni/Al-PILC does not account for this hypothesis. The reactivity (reducibility) strongly depends on the chemical nature of Me^{n+}, the cations of precious metals (Rh, Pd) being more reducible than Ni^{2+}, Ce^{4+}, as expected, and this is also verified when acidic properties are examined by ammonia desorption ($T < 300$ °C). The CO_2 reforming of methane at low temperature (650 °C) proceeds very effectively on 3% Rh and also 10% Ni catalysts, but in the latter case a high amount of carbon is deposited. The activity of catalysts can be correlated with the accessible metal surface area but no direct influence of the microstructure of the support was detected. The influence of the support seems limited to the stabilization of the metallic or oxidic sites, which in turn are responsible for catalyst activity. Compared with published data of Rh supported on different ceramic and oxide supports, 3% Rh/Al-PILC is the most active formulation.

Acknowledgements

L. Burylo, O. Gardoll, A.S. Mamède and L. Gengembre (UCCS) are thanked for XRD, thermal analyses and XPS experiments, respectively. Help from B. Revel from the NMR facility centre in Lille was greatly appreciated.

References

[1] M.C.J. Brandford, M.A. Vannice, Catal. Rev. Sci. Eng. 41 (1999) 1.
[2] J.R. Rostrup-Nielsen, Catal. Rev. Sci. Tech. 46 (2004) 247.
[3] J.-S. Chang, S.-E. Park, J.W. Yoo, J.-N. Park, J. Catal. 195 (2000) 1.
[4] J. Nakamura, K. Aikawa, K. Sato, T. Uchijima, Catal. Lett. 25 (1994) 265.
[5] J.P. Breen, R. Burch, H.M. Coleman, Appl. Catal. B: Environ. 39 (2002) 65.
[6] S. Irusta, L.M. Cornaglia, E.A. Lombardo, J. Catal. 210 (2002) 263.
[7] P. Ferreira-Aparicio, M. Fernandez-Garcia, A. Guerrero-Ruiz, I. Rodrıguez-Ramos, J. Catal. 190 (2000) 296.
[8] Z. Hou, T. Yashima, Appl. Catal. A: Gen. 261 (2004) 205.
[9] A. Djaidja, S. Libs, A. Kiennemann, A. Barama, Catal. Today 113 (2006) 194.
[10] S. Wang, G.Q.M. Lu, Appl. Catal. B: Environ. 16 (1998) 269.
[11] V.R. Choudhary, A.S. Mamman, Appl. Energ. 66 (2000) 161.
[12] H. Provendier, C. Petit, A. Kiennemann, Compte Rendus Acad. Sci. 4 (2001) 57.
[13] E. Ruckenstein, Y.H. Hu, Appl. Catal. A 133 (1995) 149.
[14] S. Hang, G.Q.M. Lu, Appl. Catal. 16 (1998) 269.
[15] B.A. Xu, J.M. Wei, Y.T. Yu, J.L. Li, Q.M. Zhu, Topics Catal. 22 (2003) 77.
[16] K. Takehira, T. Shishido, P. Wang, T. Kosaka, K. Takaki, J. Catal. 221 (2004) 43.
[17] A. Corma, A. Mifsud, P.J. Perez, Ind. Eng. Chem. Res. 27 (1988) 2044.
[18] M.S. Sun Kou, S. Mendioroz, J.L.G. Fierro, I. Rodriguez-Ramos, J.M. Palacios, A. Guerrero-Ruiz, Clays Clay Miner. 40 (1992) 167.
[19] V. Manoz, S. Mendioroz, Appl. Catal. 66 (1990) 73.
[20] M.T. Rodrigo, L. Daza, L.S. Mendioroz, Appl. Catal. 88 (1992) 101.
[21] J.A. Andersen, M.T. Rodrigo, L. Daza, S. Mendioroz, Langmuir 9 (1993) 2485.
[22] M.L. Occelli, Ind. Eng. Chem. Process Res. Dev. 22 (1983) 553.
[23] J.W.E. Coenen, Ind. Eng. Chem. Fundam. 25 (1986) 43.
[24] G.C.M. Colen, G. van Duijin, H.J. van Oosten, Appl. Catal. 43 (1988) 339.
[25] R.T. Yang, W.B. Li, J. Catal. 155 (1995) 414.
[26] L. Chmielarz, M. Zbroja, P. Kuoetrowski, B. Dudek, A. Rafalska-Łasocha, R. Dziembaj, J. Thermal Anal. Calorim. 77 (2004) 115.
[27] J. Carriazo, E. Guélou, J. Barrault, J.M. Tatibouët, R. Molina, S. Moreno, Catal. Today 107–108 (2005) 126.
[28] R. Burch (Ed.), Pillared Clays, Catal. Today 2 (1988), and papers therein.
[29] http://www.enof-mines.com.
[30] A. Gil, L. Gandia, M.A. Vicente, Catal. Rev. Sci. Eng. 42 (2000) 145.
[31] A. Samoson, E. Lippma, Phys. Rev. B, Condens. Matter 28 (1983) 6567.
[32] L. Frydman, J.S. Harwood, J. Am. Chem. Soc. 117 (1995) 5367.
[33] J.P. Amoureux, C. Fernandez, S. Steuernagel, J. Magn. Reson. 123 (1996) 116.
[34] J.P. Amoureux, C. Fernandez, Solid State Nucl. Magn. Reson. 10 (1998) 281.
[35] H. Ming-Yuan, L. Zhonghui, M. Enze, Catal. Today 2 (1988) 322.

[36] D. Plee, F. Borg, L. Gatineau, J.J. Fripiat, J. Am. Chem. Soc. 107 (1985) 2262.
[37] M.J. Hernando, C. Pesquera, C. Blanco, F. Gonzalez, Chem. Mater. 13 (2001) 2154.
[38] S.M. Bradley, R.A. Kydd, C.A. Fyfe, Inorg. Chem. 31 (1992) 1181.
[39] A. Vaccari, Catal. Today 41 (1998) 53.
[40] J.-B. d'Espinose de Lacaillerie, C. Fretigny, D. Massiot, J. Magn. Reson. 192 (2008) 244.
[41] D. Massiot, F. Fayon, M. Capron, I. King, S. Le Calvet, B. Alonso, J.-O. Durand, B. Bujoli, Z. Gan, G. Hoatson, Magn. Reson. Chem. 40 (2002) 70.
[42] M. Brotas de Carvalho, J. Pires, A.P. Carvalho, Microporous Mater. 6 (1996) 65.
[43] H.Y. Zhu, W.H. Gao, E.F. Vansant, J. Colloids Interface Sci. 171 (1995) 377.
[44] L. Storaro, M. Lenarda, R. Ganzerla, A. Rinaldi, Microporous Mater. 6 (1996) 55.
[45] L. Chmielarz, P. Kuśtrowski, M. Zbroja, B. Gil-Knap, J. Datka, R. Dziembaj, Appl. Catal. B: Environ. 53 (2004) 47.
[46] T.L. Barr, S. Seal, H. He, J. Klinowski, Vacuum 46 (1995) 1391.
[47] R.E. Grim, Clay Mineralogy, 2nd ed., Mc Graw Hill, New York, 1968.
[48] M.L. Ocelli, A. Auroux, G.J. Ray, Microporous Macroporous Mater. 39 (2000) 43.
[49] D. Zhao, Y. Yang, X. Guo, Zeolites 15 (1995) 58.
[50] G. Guiu, P. Grange, J. Catal. 168 (1997) 463.